Appl. Phys. B 69, 423–428 (1999) / Digital Object Identifier (DOI) 10.1007/s003409900188

Applied Physics B
Lasers
and Optics

Synchronously pumped femtosecond optical parametric oscillator based on $AgGaSe_2$ tunable from 2 μm to 8 μm

S. Marzenell, R. Beigang, R. Wallenstein

Fachbereich Physik, Universität Kaiserslautern, Erwin-Schrödinger-Str., D-67663 Kaiserslautern, Germany
(Fax: +49-631/205-3906, E-mail: marzenel@rhrk.uni-kl.de)

Received: 6 August 1999/Revised version: 4 October 1999/Published online: 3 November 1999

Abstract. The operation of a continuous-wave mode-locked silver gallium selenide ($AgGaSe_2$) optical parametric oscillator (OPO) is reported. The OPO was synchronously excited by 120-fs-long pulses of 1.55-μm radiation at a repetition rate of 82 MHz. The 1.55-μm radiation is generated by a non-critically phasematched cesium-titanyl-arsenate (CTA)-OPO pumped by a mode-locked Ti:sapphire laser. The $AgGaSe_2$-OPO generates signal and idler radiation in the range from 1.93 μm to 2.49 μm and from 4.1 μm to 7.9 μm, respectively. Up to 67 mW of signal wave output power has been obtained. The experimentally determined pulse duration and chirp parameters are in reasonable agreement with results from a numerical model taking into account group velocity mismatch, group velocity dispersion, self phase modulation, and chirp enhancement.

PACS: 42.65Re; 42.65Yj; 42.72Ai

There is great interest in the generation of ultrashort pulses in the mid-infrared spectral region (4 μm to 12 μm) to investigate fast transient phenomena, for example in semiconducting materials or molecules. Nonlinear frequency conversion of infrared laser light in birefringent crystals is well suited for the generation of radiation at these wavelengths. Besides difference frequency generation optical parametric oscillation generates intense radiation in the near-infrared region up to 5 μm using crystals such as KTP (and its isomorphs) or (periodically poled) $LiNbO_3$. To cover the spectral region of the mid-infrared several crystals such as $AgGaS_2$, $AgGaSe_2$, or $ZnGeP_2$ can be used [1]. Due to the broad transmission range and the large birefringence of these materials it is possible to generate radiation between 1.3 μm and 12 μm. This has been demonstrated with difference frequency generation [2–4], pulsed ns OPOs [5–10], and mode-locked ps OPOs [11, 12]. As these crystals have a band edge around 700 nm and strong two-photon absorption, it is necessary, however, to choose a pump wavelength well above 1.4 μm.

In this paper, we report what we believe to be the first demonstration of fs continuous-wave (cw) mode-locked operation of an $AgGaSe_2$-OPO in the mid-infrared spectral regime, pumped by the 1.55-μm o-polarized wave of a fs cesium-titanyl-arsenate (CTA)-OPO.

1 Experiment

A schematic layout of the cascaded OPO-system is shown in Fig. 1. A titanium sapphire laser (Spectra Physics Tsunami) generates 100-fs-long pulses around 780 nm with a repetition rate of 82 MHz and an average power of 1.7 W. This radiation is used to synchronously pump the CTA-OPO [13].

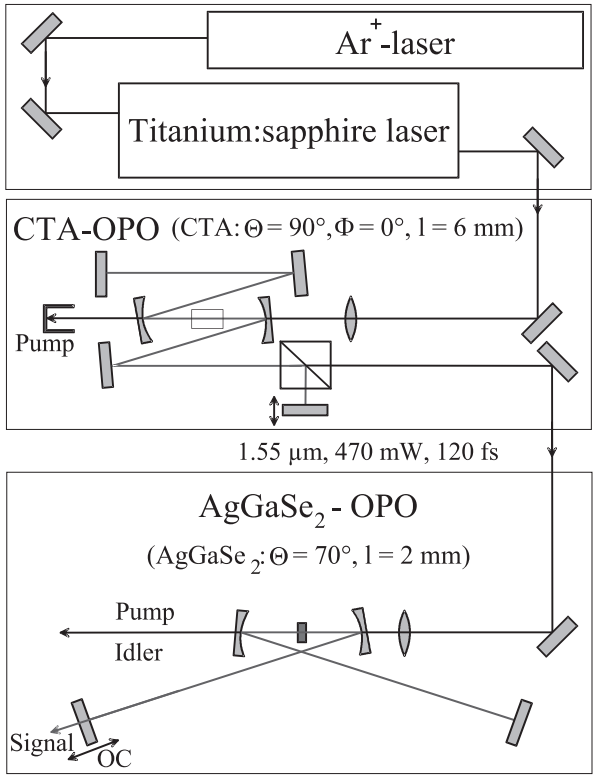

Fig. 1. Experimental setup

The CTA crystal was 6 mm long and cut for type-II phasematching ($e \rightarrow e + o$) with $\theta = 90°$ and $\phi = 0°$. The OPO is operated near the point of degeneracy [14]. It is thus of advantage to distinguish between the o- and e-polarized wave instead between the signal and idler wave. As the group velocity mismatch (GVM) between the e-polarized wave and the pump wave is in the order of 150 fs/mm, the generated e-polarized pulses are increased in pulse length to more than 350 fs. The GVM between the o-polarized wave and pump wave, on the other hand, is smaller than 25 fs/mm so that the duration of the generated o-polarized pulses is only slightly longer (by about 20%) than the pump pulses.

In order to obtain a maximum output power in the o-polarized wave (which provides the shortest pulses) it is desirable to operate the OPO with a resonator singly resonant for the e-polarized wave. However, as the OPO is operated near degeneracy both wavelengths are within the reflectivity range of the resonator mirrors. Because of the difference in group velocities the round-trip time in the resonator can be synchronized with the pump pulses for either wave by simply adjusting the cavity length. The o-polarized wave which is extracted from the cavity by a polarizing beam splitter was tunable in the range of 1.5 μm and 1.65 μm, limited only by the spectral properties of the used polarizing beam splitter. An interferometric autocorrelation of the o-polarized wave indicated chirp-free pulses with a duration of 120 fs. The generated average output power was 470 mW at 1.55 μm. This radiation was used to pump the $AgGaSe_2$-OPO.

The 1.55-μm radiation was focused by a lens ($f = 200$ mm) into the $AgGaSe_2$ crystal through one of the curved resonator mirrors (see Fig. 1). The $AgGaSe_2$ crystal ($4 \times 4 \times 2\,mm^3$) was cut for type-I phasematching ($e \rightarrow o + o$) with $\theta = 70°$. Because of the small walk-off angle of 0.4° between signal and the pump wave, collinear pumping was applied. The signal resonant cavity of the $AgGaSe_2$-OPO consisted of two spherical mirrors with a radius of curvature of 75 mm and two plane mirrors which defined a beam waist $\omega_0 = 25$ μm at the center of the crystal.

For practical reasons the wavelength of the CTA-OPO was first tuned to 1.58 μm. This radiation was used to align the resonator of the $AgGaSe_2$-OPO, as at this wavelength the residual reflectivity of the resonator mirrors was sufficient for this purpose. After alignment of the mirrors the adjustment of the resonator length to the repetition rate of the pump source started the oscillation of the $AgGaSe_2$-OPO. The OPO output was detected with a lead sulphide detector. A germanium filter in front of the detector blocked the residual pump radiation.

2 Wavelength tuning

Tuning of the $AgGaSe_2$-OPO can be accomplished either by using a fixed pump wavelength from the CTA-OPO and rotating the $AgGaSe_2$ crystal, or by keeping a fixed crystal angle and changing the pump wavelength by changing the titanium:sapphire wavelength. This is illustrated in Fig. 2. The solid lines are the phasematching curves calculated with the Sellmeier equations from Komine et al. [15]. If, for example, the wavelength of the CTA-OPO is changed between 1.49 μm and 1.6 μm a $AgGaSe_2$ phasematching angle of 70° provides wavelengths between 2 μm and 2.5 μm for the signal wave

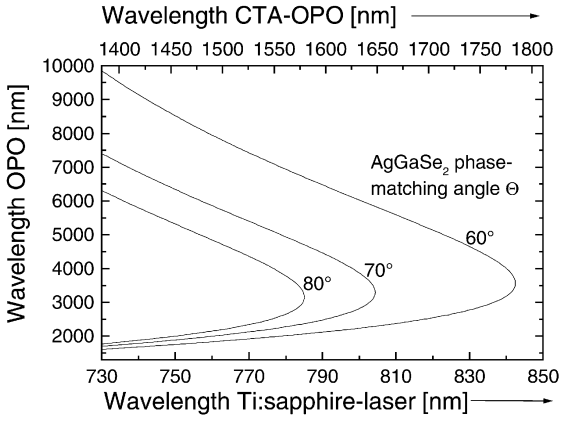

Fig. 2. Phasematching curve of the $AgGaSe_2$-OPO pumped by a CTA-OPO calculated with the Sellmeier equations

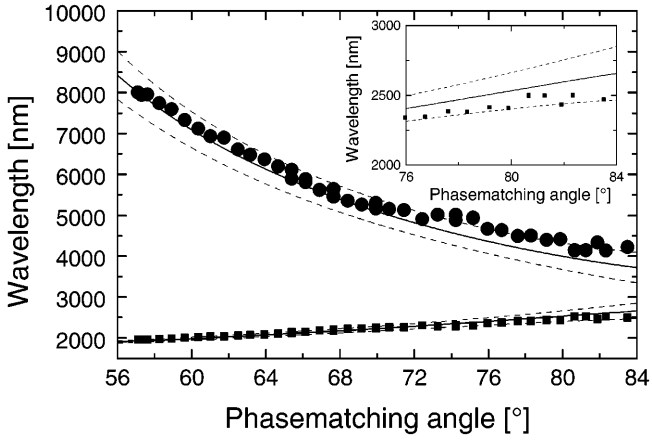

Fig. 3. Wavelength of the signal and idler radiation of the $AgGaSe_2$-OPO pumped by 1.55-μm CTA-OPO radiation. The *solid curve* is calculated with the Sellmeier equations. The *dashed curves* are the limits of the corresponding spectral acceptance bandwidths. The *insert* shows in more detail the signal wave at large phasematching angles

and between 4.4 μm and 5.9 μm for the idler wave. With a fixed CTA wavelength of 1.55 μm a variation of the phasematching angle between 60° and 80° tunes the OPO wavelength in the range of 2 μm and 2.5 μm for the signal wave and 4 μm and 7 μm for the idler wave. It is of course possible to use a combination of these two techniques to choose almost any desirable combination of two wavelengths from the CTA-OPO and $AgGaSe_2$-OPO.

In our experiment the wavelength from the CTA-OPO was fixed at 1.55 μm and the wavelength tuning of the $AgGaSe_2$-OPO was accomplished by rotating the crystal. In Fig. 3 the measured crystal angle and the wavelengths of the signal and idler waves are plotted together with the values calculated from the known Sellmeier equations [15]. The limits of the spectral acceptance bandwidth for both waves are indicated with dashed lines. The signal wave was tuned from 1.93 μm to 2.49 μm and the corresponding idler wave from 4.1 μm to 7.9 μm with two mirror sets. The insert shows in more detail the measured wavelengths of the signal wave together with the calculated data at large phasematching angles. For these angles the wavelength of the signal wave remains almost constant and differs significantly from the calculated values. This

difference can be explained by water vapor absorption in the air which results in additional losses for the signal wave at longer wavelengths. Because of the large spectral acceptance bandwidth the signal wave is shifted to shorter wavelengths where the OPO operates with smaller losses. Furthermore, higher losses due to the increasing transmission of the used resonator mirrors, and the astigmatism due to the large external angle of the crystal, limited the tuning range.

3 Threshold

Together with the measurement of the generated signal and idler wavelengths the pump power at threshold was measured in dependence of the phasematching angle. The measured values are plotted in Fig. 4 as a function of the signal wavelength. The experimentally determined pump powers at threshold are compared with those calculated using the theory of McCarthy and Hanna [16] which are plotted as a solid line. The losses are assumed to be 5.95% and consist of 2.0% output coupler loss and 3.95% additional losses resulting from losses at the crystal surfaces and the resonator mirrors. The calculated threshold increases from 2500 nm to 1900 nm due to a 28% decrease of the figure of merit (FOM) and an increasing walk-off angle which results in a 10% reduction of the interaction length inside the crystal. The differences between the measured and the theoretically calculated threshold values (observed below 2.0 μm and above 2.4 μm) can be explained by water vapor absorption in the air and higher transmission losses of the resonator mirrors at the lower and upper limit of the tuning range.

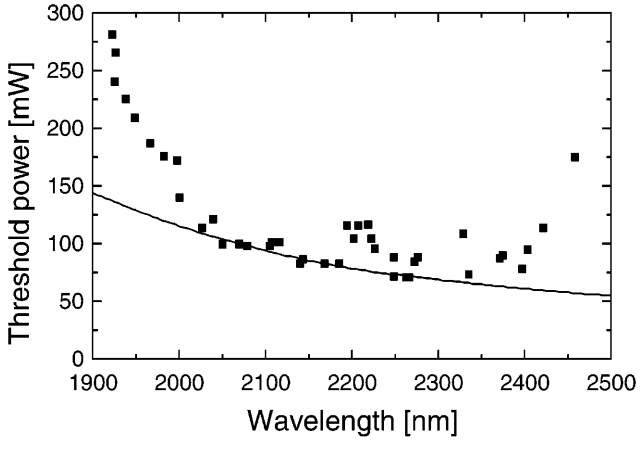

Fig. 4. Threshold power of the $AgGaSe_2$-OPO as a function of the signal wavelength

4 Output powers

In order to prevent damage of the $AgGaSe_2$-crystal during the alignment of the OPO, the pump beam was mechanically chopped with a duty cycle of 1 : 7. The pump beam was also chopped during the measurements of the tuning range. The chopper was removed for the measurements of the output power. Figure 5 shows the average output power of the signal and idler wave as a function of wavelength. Two mirror sets were used to cover the range from 1.95 μm to 2.55 μm of the resonant signal wave. The maximum average signal output power of 26 mW was measured at 2.2 μm. The idler power exceeded 22 mW at 5.25 μm. The idler wave is partly absorbed by CO_2 at 4.25 μm and H_2O vapor which has a broad absorption band that is centered at 6.27 μm but extends from 5.0 μm to 7.5 μm. As the idler wave is nonresonant the threshold is not influenced by this absorption. All these measurements were performed with a 2.0% output coupler in order to have low threshold power and small losses which allows for a large tuning range. To increase the power of the signal wave, and to study the pump power at threshold and the slope efficiency, three different output couplers were used.

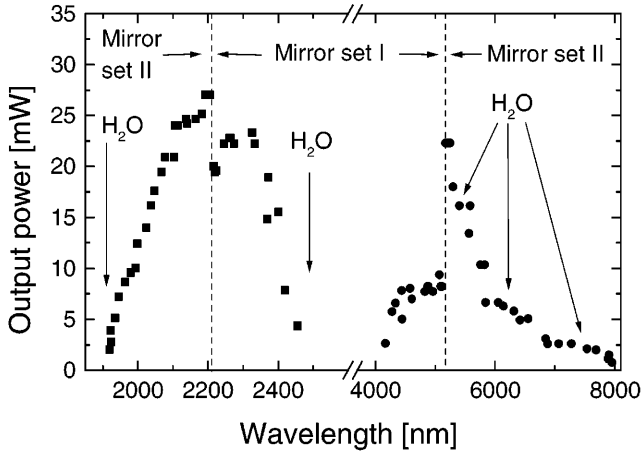

Fig. 5. Wavelength dependence of the output power of signal and idler wave of the $AgGaSe_2$-OPO

The average output power of the signal wave at 2.35 μm as a function of the pump power for the three different output couplers is shown in Fig. 6. The values of the pump power given in Fig. 6 represent the pump power present inside the $AgGaSe_2$ crystal. The pump power from the CTA-OPO is reduced by the losses at the turning mirrors, the focusing lens, the first curved mirror, and one surface of the crystal. Due to these losses the output power of the CTA-OPO was reduced to 403 mW. The thresholds determined from the measurements (shown in Fig. 6) are in good agreement with calcu-

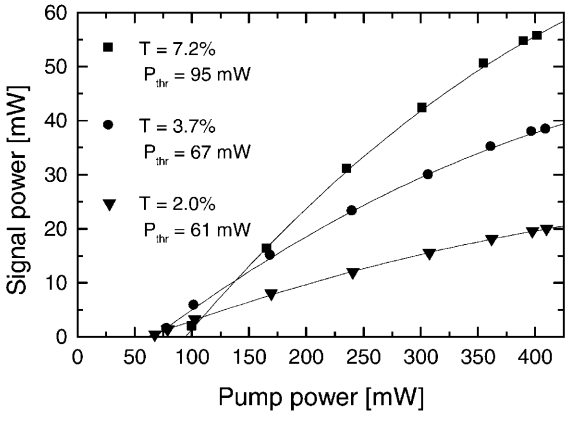

Fig. 6. Output power of the signal wave as a function of the pump power for three different ouput couplers

lated values taking into account the transmission of the output couplers and assuming additional internal losses of 3.95%. The idler wave experienced a power loss of 29% as a result of reflectivity losses at the crystal facets, the reflectivity of the second curved mirror, and the losses at the CaF_2 lens. With a pump power inside the crystal of 403 mW and an output coupler with 7.2% transmission an average output power of 67 mW and 35 mW was measured for the signal and idler wave, respectively. The external efficiency was 13.9% with a slope efficiency of 18.1%. The measured pump depletion of 40% indicates that 161 mW of the pump power was converted into signal and idler power. Using the Manley–Rowe relation, this corresponds to 108 mW signal and 53 mW idler power. Taking into account the additional losses of 3.95% for the signal wave and 29% for the idler wave, these values are in good agreement with the measured total average power.

5 Pulse measurements

To understand the processes that influence the pulse formation in the $AgGaSe_2$-OPO, interferometric autocorrelations for both waves were performed simultaneously to determine pulse length and pulse chirp. The signal wave at 2.4 μm is frequency doubled in a $5 \times 5 \times 1\,\mathrm{mm}^3$ BBO crystal cut at $\theta = 20°$. The second harmonic is detected with a germanium diode. Frequency doubling of the idler wave is obtained in a $5 \times 5 \times 2\,\mathrm{mm}^3$ $AgGaSe_2$ crystal cut at $\theta = 46°$ and the second harmonic is detected with a lead sulphide detector.

To analyse the measured interferometric autocorrelations and to determine the pulse length and chirp a Gaussian pulse shape was assumed:

$$E(t) = E_0 \exp\left(-\frac{t^2}{2T^2}\right) \cos\left(\omega t + \frac{at^2}{T^2}\right) .$$

The parameter T is related to the full width at half maximum of the pulse duration $\tau(\tau_{\mathrm{FWHM}} = 2\sqrt{2\ln 2} \times T)$. The parameter a describes the amount of a linear chirp. Using this pulse shape the calculated autocorrelation function $g_{\mathrm{B}}^2(\tau)$ [17] was fitted to the measurements.

The output power and pulse parameters (duration and chirp) critically depend on the resonator length of the OPO. Therefore for the following measurements the resonator length was always adjusted to obtain the maximum signal output power. The pulse properties were first investigated as a function of intracavity peak pulse power of the signal wave. The intracavity peak power of the signal wave was altered by changing the output coupler and/or changing the pump power. With the 7.2% output coupler and a reduced pump power of 350 mW (instead of 470 mW) in front of the focusing lens, the intracavity peak power of the resonant signal wave was 15 kW. With this intracavity pulse power, signal pulses with 400 fs duration and a chirp factor of 1.45 were obtained at 2.4 μm (see Fig. 7). If the transmission of the output coupler is reduced to 2.0% and the maximum available pump power of 470 mW is used, then the intracavity peak power increases to 30 kW which results in a pulse length of 480 fs with a chirp factor of 2.35 as shown in Fig. 8.

In contrast to the signal wave, the pulse length of the idler wave ($\lambda = 4.7$ μm) remains almost constant and is between 490 fs and 460 fs. Also the chirp remains constant

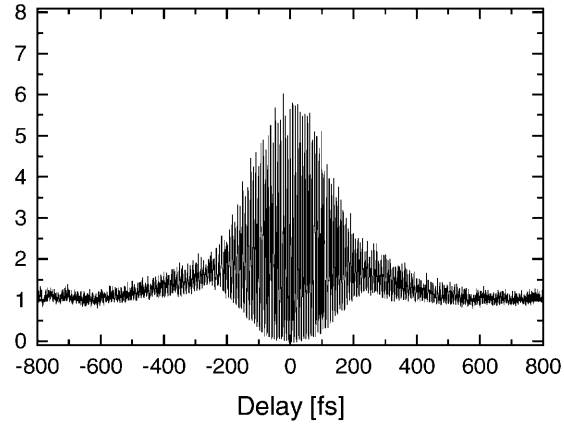

Fig. 7. Interferometric autocorrelation of the signal pulses at 2.4 μm with an intracavity peak power of 15 kW ($\tau = 400$ fs, $a = 1.45$)

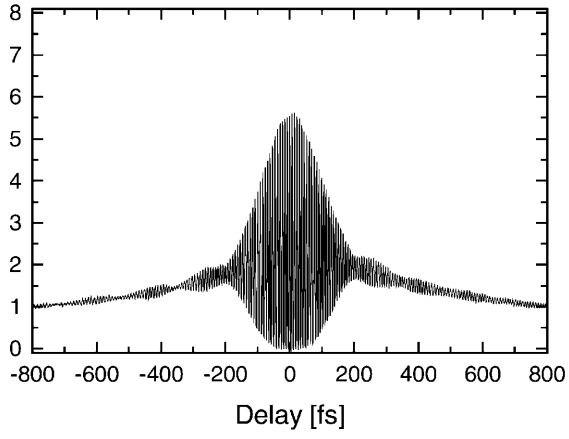

Fig. 8. Interferometric autocorrelation of the signal pulses at 2.4 μm with an intracavity peak power of 30 kW ($\tau = 480$ fs, $a = 2.35$)

($a \approx 1$). The autocorrelation measurements for the idler wave are shown for an intracavity peak power of 15 kW in Fig. 9 and for the maximum intracavity peak power of 30 kW in Fig. 10. From these interferometric autocorrelation measure-

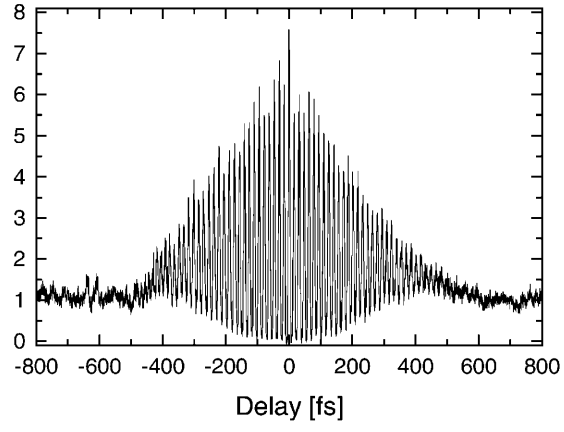

Fig. 9. Interferometric autocorrelation of the idler pulses at 4.7 μm with an intracavity peak power of 15 kW ($\tau = 490$ fs, $a = 1$)

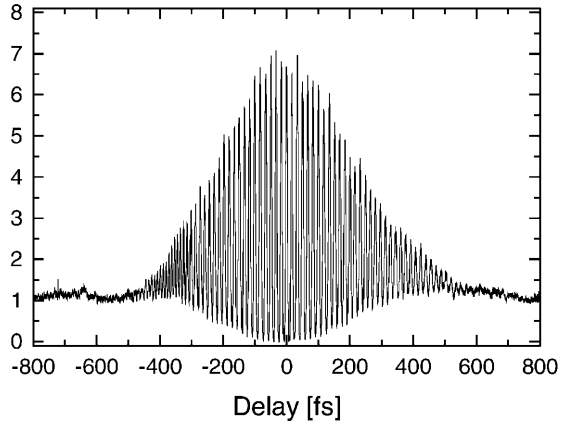

Fig. 10. Interferometric autocorrelation of the idler pulses at 4.7 μm with an intracavity peak power of 30 kW ($\tau = 460$ fs, $a = 1$)

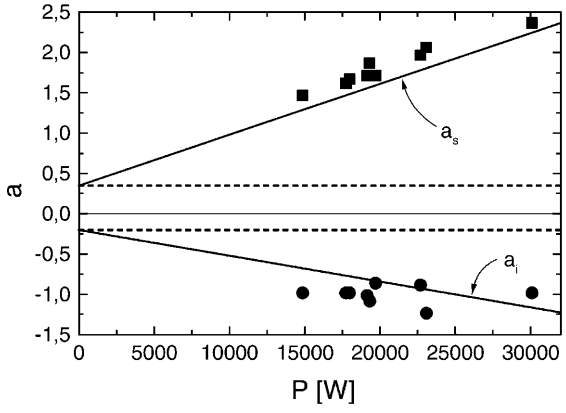

Fig. 11. Chirp of signal and idler wave as a function of the resonator internal signal power. For details see text

ments it is obvious that signal and idler pulses have a strong chirp even without a chirp on the pump pulse.

The chirp factors of signal and idler wave are shown in Fig. 11 as a function of the intracavity peak power of the resonant signal wave. The strong increase in pulse length and chirp of the signal wave with increasing intracavity power is explained in terms of a chirped pump pulse together with chirp enhancement and self phase modulation due to the high intracavity peak power:

The pump pulse experiences a chirp due to group velocity dispersion of the lens material and the $AgGaSe_2$ crystal itself. Taking only into account the group velocity dispersion in the 2-mm $AgGaSe_2$ crystal, the pump pulse experiences a linear chirp of $a = 0.15$. As the spectral properties of the pump pulse influence the spectral properties of signal and idler pulses in a phasematched parametric frequency conversion process, a chirped pump pulse leads to chirped signal and idler pulses. The generated chirps can be calculated using the phasematching conditions (conservation of energy $\omega_s + \omega_i = \omega_p$ and momentum $\boldsymbol{k}_s + \boldsymbol{k}_i = \boldsymbol{k}_p$) and taking into account additional time-dependent frequency terms $\omega + \dot{\phi}(t)$ which depend on the chirp of the pump pulse [18]. The calculation leads to factors between the time derivatives of the phases for signal, idler, and pump wave: $\dot{\phi}_s = p_s \dot{\phi}_p$ and $\dot{\phi}_i = p_i \dot{\phi}_p$. The factors p_s and p_i only depend on $d\omega/dk$ (i.e. the shape of the phasematching curve). If $|p_s|, |p_i| > 1$, then the chirp of signal and idler pulses can be stronger than the pump chirp. This is the case for $AgGaSe_2$, where $p_s = 2.5$ for the signal wave at 2.4 μm and $p_i = -1.5$ for the idler wave at 4.7 μm. This results in a residual chirp of $a_{0s} = 0.35$ for the signal wave and $a_{0i} = -0.2$ for the idler wave. These values are independent of the resonator internal peak power. These residual chirps are marked in Fig. 11 by the horizontal dashed lines. In addition, the chirp of the signal pulses increases with increasing intracavity peak power of the signal wave caused by self phase modulation. This increase of the chirp is calculated with [19]:

$$a = a_{0s} + \frac{n^{(nl)} \times q \times l_c \times \tau^2}{\lambda_0 \times w_{eff}^2 \times \ln(2)} \times P \,.$$

Here q is the lifetime of the pulses inside the resonator measured in round-trip times, l_c is the crystal length, τ the pulse length, λ_0 the wavelength, w_{eff} the beam waist, and P the intracavity peak power. To determine the nonlinear refractive index $n^{(nl)}$ of $AgGaSe_2$ a Z-scan measurement [20] was performed. From this measurement the nonlinear refractive index of $AgGaSe_2$ was determined to be $n^{(nl)} = 350 \times 10^{-16}$ cm^2/W. The lifetime of the pulses inside the resonator is assumed to be 10 round-trip times. This value was estimated from the losses of the output coupler and from the additional losses at the other resonator internal components. Together with the residual chirp we obtain for the signal wave the chirp a_s shown in Fig. 11 as the solid line with positive slope.

Although the idler wave itself experiences no significant self phase modulation as the idler wave is not resonant, self phase modulation of the signal wave is transferred to the idler wave via phasematching. Because of the negative sign of the chirp enhancement factor p_i the chirp of the idler wave has the opposite sign. Its magnitude increases with increasing intracavity signal power. In addition, cross phase modulation due to the high intracavity peak power of the signal wave influences the idler wave. As the cross phase modulation has a positive sign and increases with increasing intracavity power the negative slope of the idler chirp is reduced. Together with the residual chirp this leads to a calculated chirp a_i of the idler wave represented in Fig. 11 by the solid line with negative slope. The calculated dependence and the experimentally determined variation of the chirp values a_s and a_i as a function of intracavity power are in reasonable agreement.

To get bandwidth-limited pulses from the $AgGaSe_2$-OPO it is necessary to compress the pulses outside the resonator for both waves seperately or inside the resonator for the resonant signal wave. According to the measured chirp and pulse length it should be possible to compress the signal pulses down to 100 fs and the idler pulses to 150 fs. All these measurements were done in a resonator configuration adjusted to maximum signal output power. If the resonator configuration is changed to obtain maximum idler output power then the pulse lengths are shorter ($\tau = 305$ fs) and the chirp decreases ($a = 0.3$) as it is shown in Fig. 12. The reason for this phenomenon is a different resonator round-trip time with reduced intracavity signal power. Therefore self phase modulation is decreased and also the interaction length between pump, signal, and idler wave inside the crystal is influenced. With a negative chirp factor $p_i = -1.5$ for the idler wave

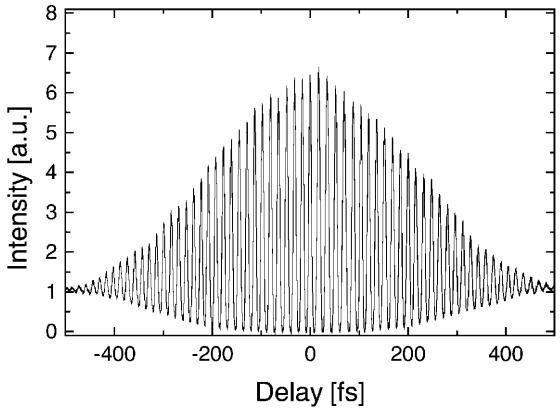

Fig. 12. Interferometric autocorrelation of the idler pulses at 4.8 μm with a resonator configuration adjusted to maximum idler output power ($\tau =$ 305 fs, $a = 0.3$)

and a positive group velocity dispersion for both OPO waves ($\approx 400\ \mathrm{fs}^2/\mathrm{mm}$ for the signal wave and $\approx 100\ \mathrm{fs}^2/\mathrm{mm}$ for the idler wave), the idler pulse is partly self-compressed by the $AgGaSe_2$ crystal [21]. To understand these effects in detail, a numerical simulation is in progress, at present.

6 Summary

We have demonstrated continuous-wave mode-locked operation of an OPO based on $AgGaSe_2$. The OPO was pumped with the o-polarized 1.55-μm radiation of a cw modelocked, noncritically phasematched, titanium-sapphire laser-pumped CTA-OPO. The pump wavelength ensures a reduced two-photon absorption in the $AgGaSe_2$ crystal. Femtosecond pulses were generated in the mid-infrared between 1.93 μm and 2.49 μm for the signal wave, and between 4.1 μm and 7.9 μm for the idler wave. Average output powers as high as 67 mW and 35 mW for signal and idler wave, respectively, were obtained. The signal and idler pulses were characterized by measuring the corresponding interferometric autocorrelations. Pulse lengths of signal and idler pulses were measured to be between 230 fs to 520 fs and 300 fs to 640 fs, respectively, depending on the pump power, output coupling, and resonator alignment. The variation of pulse durations and chirp factors of signal and idler pulses was explained in terms of a combination of self phase modulation, cross phase modulation, and chirp enhancement caused by a chirp of the pump pulse. For the calculation of self and cross phase modulation the nonlinear refractive index of $AgGaSe_2$ was measured using the Z-scan method.

References

1. P.G. Schunemann, K.L. Schepler, P.A. Budni: MRS Bulletin **23**, 45 (1998)
2. M.R.X. de Barros, R.S. Miranda, T.M. Jedju, P.C. Becker: Opt. Lett. **20**, 481 (1995)
3. J. Hong, A.D.O. Bawagan, S. Charbonneau, A. Stolow: Appl. Opt. **36**, 1894 (1997)
4. J.M. Fraser, D. Wang, A. Haché, G.R. Allan, H.M. van Driel: Appl. Opt. **36**, 5044 (1997)
5. R.C. Eckardt, Y.X. Fan, R.L. Byer, C.L. Marquardt, M.E. Storm, L. Esterowitz: Appl. Phys. Lett. **49**, 608 (1986)
6. N.P. Barnes, D.J. Gettemy, J.R. Hietanen,R.A. Iannini: Appl. Opt. **28**, 5162 (1989)
7. P.A. Budni, P.G. Schunemann, M.G. Knights, T.M. Pollak, E.P. Chicklis: OSA Proc. Adv. Solid State Lasers Conf. **13**, 380 (1992)
8. P.A. Budni, M.G. Knights, E.P. Chicklis, K.L. Schepler: Opt. Lett. **18**, 1068 (1993)
9. N.P. Barnes, K.E. Murray, M.G. Jani, S.R. Harrell: J. Opt. Soc. Am. B **11**, 2422 (1994)
10. J. Kirton: Opt. Commun. **115**, 93 (1995)
11. E.C. Cheung, K. Koch, G.T. Moore: Opt. Lett. **19**, 631 (1994)
12. C. Grässer, S. Marzenell, J. Dörring, R. Beigang, R. Wallenstein: OSA TOPS **1**, 158 (1996)
13. S. Marzenell, R. Beigang, R. Wallenstein: In *Ultrafast Phenomena XI*, ed. by T. Elsaesser, J.G. Fujimoto, D.A. Wiersma, W. Zinth, Proceedings of the 11th International Conference, Garmisch-Partenkirchen, Germany, July 12–17, 1998 (Springer, Berlin, Heidelberg 1998) p. 63
14. B. Köhler, J. Dörring, A. Nebel, R. Wallenstein: Paper CThN2 in Conference on Lasers and Electro-Optics Europe, IEEE Technical Digest (Institute of Electronical and Electronics Engineers, Piscataway 1996) p. 303
15. H. Komine, J. M. Fukumoto, W. H. Long, E. A. Stappaerts: IEEE STQE **1**, 44 (1995)
16. M.J. McCarthy, D.C. Hanna: J. Opt. Soc. Am. B **10**(11), 2180 (1993)
17. K.L. Sala, G.A. Kenney-Wallace, G.E. Hall: IEEE J. Quantum Electron. **QE-16**(9), 990 (1980)
18. A. Piskarskas, A. Stabinis, A. Yankauskas: Sov. J. Quantum Electron. **15**(9), 1179 (1985)
19. G.P. Agrawal: *Nonlinear Fiber Optics* (Academic Press, S Diego, London 1995)
20. M. Sheik-Bahae, A.A. Said, T.-H. Wei, D.J. Hagan, E.W. van Stryland: IEEE J. Quantum Electron. **QE-26**(4), 760 (1990)
21. R. Laenen, H. Graener, A. Laubereau: J. Opt. Soc. Am. B **8**(5), 1085 (1991)